CHEMISTRY OF MATERIALS

pubs.acs.org/cm

Article

Ultra-Broad-Band-Excitable Cu(I)-Based Organometallic Halide with Near-Unity Emission for Light-Emitting Diode Applications

Jinglong Huang,[⊥] Binbin Su,[⊥] Enhai Song, Maxim S. Molokeev, and Zhiguo Xia*

Cite This: *Chem. Mater.* 2021, 33, 4382−4389

Read Online

ACCESS | Metrics & More | Article Recommendations | Supporting Information

ABSTRACT: Low-dimensional hybrid metal halides demonstrate broad-band emission and high photoluminescence quantum yield (PLQY) acting as excellent candidates for a new generation of luminescent materials in lighting fields. However, most luminescent metal halides can only be excited by ultraviolet radiation, and the discovery of high-efficient emitters with broad-band excitation characteristics, especially upon efficient blue light irradiation, is a challenge. Herein, a zero-dimensional (0D) Cu(I)-based organometallic halide (18-crown-6)$_2$Na$_2$(H$_2$O)$_3$Cu$_4$I$_6$ (CNCI) was prepared with a green emission band centered at 536 nm and a near-unity PLQY (91.8%) upon excitation of 450 nm. Importantly, the ultrabroad excitation band covering a 300−500 nm range was observed in CNCI, and the luminescence mechanism has been discussed in detail. A white light-emitting diode (WLED) was fabricated with high luminous efficiency of 156 lm/W and a high color rendering index of 89.6. This work provides guidance for designing high-performance luminescent metal halides with suitable excitation characteristics and also promotes the application prospects of such materials in WLED fields.

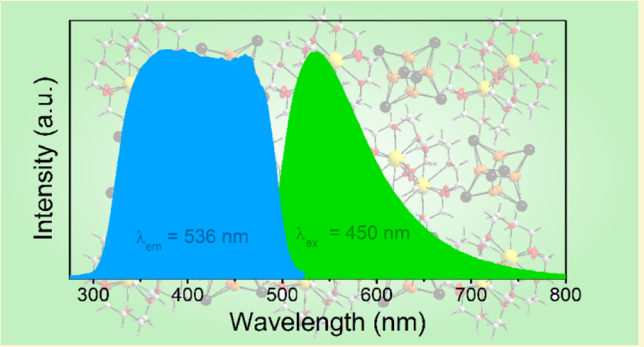

INTRODUCTION

White light-emitting diodes (WLEDs) have revolutionized modern lighting sources, with the advantages of low-voltage power supply, low-energy consumption, high stability, short response time, no pollution to the environment, multicolor light emission, and so on.[1] Herein, utilization of blue LED chips plays a significant role in the fabrication of WLEDs because of their high efficiency and low cost.[2] Thus, the discovery of new luminescence materials beyond rare earth phosphors such as $Y_3Al_5O_{12}:Ce^{3+}$, which can be efficiently pumped by blue light, is a hot topic.[3] As an emerging family of luminescence materials, molecular-level low-dimensional metal halide perovskites have received growing attention in recent years due to their impressive structural diversity, excellent optical properties, and enormous application prospects in the fields of LED,[4] solar cells,[5] and photodetectors.[6]

Considering the exploration of multicolor emitters for WLEDs, it is crucial to design superior yellow-green-emitting luminescence materials in metal halides with appropriate peak bandwidth, high photoluminescence quantum yield (PLQY), and excellent stability to meet the needs for industrial applications.[7] To date, most of the reported high-efficient yellow-green light-emission metal halide materials that can be excited by blue light are concentrated in Mn(II)-based compounds.[8,9] However, Mn(II)-based metal halides usually suffer from poor stability against moisture and heat, and, especially, the typical *d*−*d* transition emission mode is arduous to be regulated. It is a challenge to find metal halide emitters with ultra-broad-band-excitable characteristics.

Due to the advantages of earth abundance, low toxicity, and low cost, copper (Cu)-based functional material has become a suitable choice to form Cu(I)-based metal halides.[10,11] Recently, Hosono and co-workers first reported $Cs_3Cu_2I_5$ with efficient blue emission, which triggered the exploration of Cu(I)-based metal halide luminescence materials.[12] However, despite highly efficient blue/green emission, the suboptimal excitation peak position (~300 nm) of the reported all-inorganic Cu^+-based metal halides greatly restricted their further commercial applications.[13−15] Besides, organic−inorganic hybrid metal halides are an interesting family of functional materials with impressive structural diversity and enormous application prospects.[2,16,17] Unlike inorganic solids, the organic−inorganic hybrid metal halides allow us to artificially design the connectivity of an inorganic lattice by choosing suitable organic components.[18−20] For example, Li et al. reported a lead-free Cu(I)-based organic−inorganic perovskite-related material $[K(C_8H_{16}O_4)_2]_2[Cu_4I_6]$

Received: January 10, 2021
Revised: May 18, 2021
Published: June 2, 2021

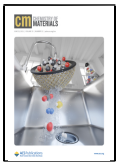

Downloaded via STATE PUBLIC SCITECH LIBRARY SB RAS on November 8, 2021 at 05:26:40 (UTC).
See https://pubs.acs.org/sharingguidelines for options on how to legitimately share published articles.

ACS Publications

© 2021 American Chemical Society

https://doi.org/10.1021/acs.chemmater.1c00085
Chem. Mater. 2021, 33, 4382−4389

with one-dimensional (1D) clusters, which exhibits greenish-yellow emission (545 nm) with a near-unity PLQY (~97.8%).[21] However, the photoluminescence excitation (PLE) spectrum shows that blue light is still not located in the optimal excitation region.

To meet commercial LED applications, a 0D Cu(I)-based organometallic halide using crown-ether as the organic component is reported herein. For this compound, crown-ether coordinates with Na^+ to form complex cations, which are assembled with special $Cu_4I_6^{2-}$ to form the compound $(18\text{-crown-6})_2Na_2(H_2O)_3Cu_4I_6$ (CNCI) with a 0D structure. It is noticed that the crystal structure has been previously reported by Nurtaeva et al. in 1999, and emission at 520 nm under 300 nm excitation was observed,[22] which promotes the development of Cu(I)-based organometallic halides. Based on these pioneer discoveries, we further explore the photophysical properties and analyze the luminescence mechanisms of CNCI in this work. Herein, the optical properties of CNCI were examined in detail, in which a broad-band green asymmetric emission centered at 536 nm with a near-unity PLQY was investigated. An ultra-broad-band excitation peak with a plateau covering a 300−500 nm range and the excellent chemical and moisture stability also enable its further applications for solid-state lighting. The detailed optical characterizations demonstrate that the asymmetric emission is dual luminescence corresponding to two different energy states, and a metal-to-ligand charge transfer or a halide-to-ligand charge transfer (MLCT/HLCT) excited state leads to high-energy emission at 536 nm and a cluster-centered (CC) excited state leads to low-energy emission at 700 nm. Considering the unique optical performance and excellent stability of CNCI, we finally demonstrated the potential application of CNCI in a WLED. This work aims at providing guidance for the design and development of ultra-broad-band-excited low-dimensional luminescent metal halide materials in the future.

EXPERIMENTAL SECTION

Reagents. Copper(I) iodide (CuI, 98%), sodium iodide (NaI, 99%), 18-crown-6 ($C_{12}H_{24}O_6$, 99%), hypophosphorous acid (H_3PO_2, 50% in water by weight), and acetone (C_3H_6O, 99.5%) were purchased from Aladdin. All chemicals were used as received.

Synthesis. For the synthesis of the CNCI single crystal, 18-crown-6 (2.5 mmol), NaI (2.5 mmol), CuI (2.5 mmol), and H_3PO_2 (5 mL) were first dissolved in acetone (15 mL) at room temperature with stirring to form a clear solution. Then, large-sized crystals were obtained by slowly evaporating the solvent at room temperature for a few days. Powder crystals were obtained by evaporating the solvent at 60 °C for less than 30 min.

Characterization. Single-crystal X-ray diffraction (SCXRD) was conducted on a SMART APEX II X-ray single-crystal diffractometer (Bruker AXS, analytical equipment of Krasnoyarsk Center of collective use of SB RAS) equipped with a CCD detector, a graphite monochromator, and a Mo Kα radiation source (λ = 1.5406 Å) at 150 K. The absorption corrections were applied using the SADABS program. The structures were solved by the direct methods using package SHELXS and refined using the SHELXL program.[23] All of the hydrogen atoms of the $C_{12}H_{24}O_6$ ligand were positioned geometrically as riding on their parent atoms with d(C−H) = 0.97 Å for the C−H bonds and Uiso(H) = 1.2 Ueq(C, N). The structural tests for missing symmetry elements and possible voids were conducted using the PLATON program.[24] Powder X-ray diffraction (PXRD) measurement was performed on an Aeris PXRD diffractometer (PANalytical Corporation, the Netherlands) operating at 40 kV and 15 mA with monochromatized Cu Kα radiation (λ = 1.5406 Å). Rietveld structure refinements were performed by TOPAS 4.2.[25] The absorption spectrum was collected using a UV−vis−NIR spectrophotometer (Hitachi Corporation, UH4150) at room temperature, in which $BaSO_4$ was used as the reference standard. The photoluminescence excitation (PLE) and photoluminescence (PL) emission spectra were obtained on an FLS1000 fluorescence spectrophotometer (Edinburgh Instruments Ltd., U.K.). The PLQY was measured using an absolute PL quantum yield spectrometer (Hamamatsu, C13534). The lifetimes were measured on an Edinburgh FLS1000 fluorescence spectrometer. The dynamics of emission decay was monitored using the FLS1000s time-correlated single-photon counting capability (1024 channels; 1 μs window) with data collection for 5000 counts in the maximum channel. The WLED was fabricated using a blue GaN chip (λ_{em} = 450 nm) as the excitation source, while CNCI and KSF/Mn^{4+} were used as the green phosphor and the red phosphor, respectively. The proper amounts of phosphors were thoroughly mixed with epoxy resin, and the obtained mixtures were coated on an LED chip. The photoelectric properties, including the PL spectra, correlated color temperature (CCT), color rendering index (R_a), and CIE color coordinates of WLEDs, were tested using an integrating sphere spectroradiometer system (ATA100, Everfine).

RESULTS AND DISCUSSION

The as-grown CNCI crystal belongs to the monoclinic space group $P2_1/c$ with lattice parameters of a = 10.7308(3) Å, b = 14.41940(4) Å, and c = 8.50350(2) Å. The crystallographic information file (CIF) of CNCI is provided in the Supporting Information (SI), the main crystallographic data and analysis parameters are given in Tables 1 and S1, respectively, and the fractional atomic coordinates and isotropic or equivalent isotropic displacement parameters are shown in Table S2. Rietveld refinement of the powder pattern of the ground CNCI powder is shown in Figure S1, which is in good agreement with the calculated data based on the single-crystal structure data of CNCI and previous reports.

Table 1. Main Crystal Structure Parameters of CNCI Single Crystal

chemical formula	$C_{24}H_{54}Cu_4I_6Na_2O_{15}$
abbreviation	CNCI
molecular weight	1644.19
temperature (K)	293
crystal system	monoclinic
space group, Z	$P2_1/c$, 2
a (Å)	11.2186 (3)
b (Å)	13.7976 (4)
c (Å)	15.2854 (4)
α (°)	90
β (°)	96.979(2)
γ (°)	90
V (Å^3)	2348.49 (11)
ρ_{calc} (g/cm^3)	2.322
$2\theta_{max}$ (°)	57.39
$R1$ [$F_o > 4\sigma(F_o)$]	0.0236
$wR2$	0.0500
Goof	0.950

In CNCI, the 18-crown-6 ether coordinates alkali metal or alkaline earth metal readily[26−28] so that Na^+ coordinates with 18-crown-6 and two crown-ether metal complexes are connected by two H_2O molecules, and the detailed crystal information is given in Figure 1. As shown in Figure 1a, it should be noted that though there are two H_2O sites between the crown-ether metal complexes, only 50% are occupied,

https://doi.org/10.1021/acs.chemmater.1c00085
Chem. Mater. 2021, 33, 4382−4389

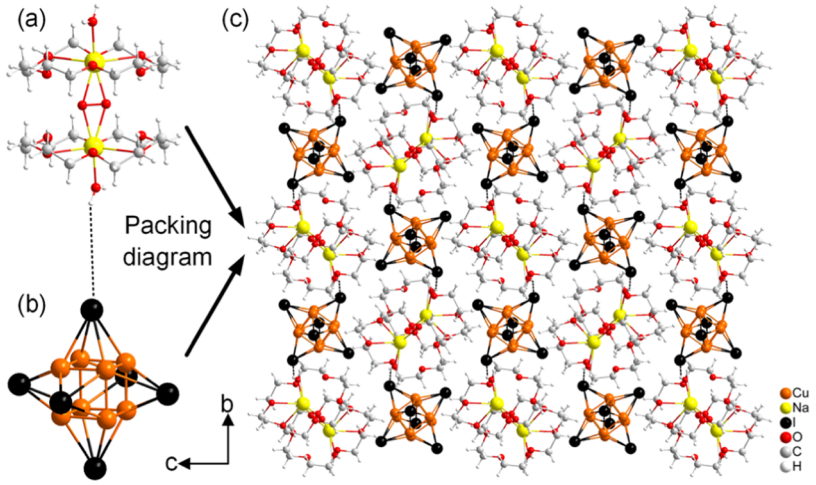

Figure 1. (a) Detailed view of $(18\text{-crown-6})_2Na_2(H_2O)_3^{2+}$ ions. Each Na ion is coordinated by one 18-crown-6 organic ligand and two H_2O molecules placed in the poles, forming a block. Two such blocks are joined with each other through a H_2O bridge molecule, which is disordered over two sites. The disordered H_2O molecule is depicted without H atoms since they were not localized. (b) Detailed view of $Cu_4I_6^{2-}$ polyhedral units. The four Cu^+ ions are disordered over eight sites in the structure; thus, they occupy sites only with 50% probability. (c) Crystal structure of $(18\text{-crown-6})_2Na_2(H_2O)_3Cu_4I_6$ viewed along the *a*-axis to show the 0D character with isolated $Cu_4I_6^{2-}$ units.

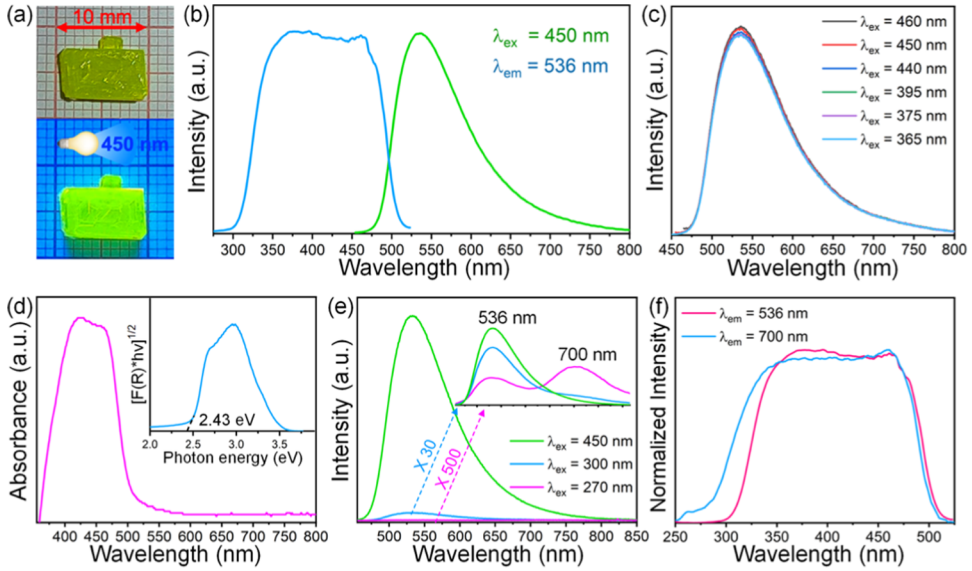

Figure 2. (a) Optical photograph of the as-grown CNCI single crystals under daylight (top) and 450 nm blue light (down). (b) PL (λ_{ex} = 450 nm) and PLE (λ_{em} = 536 nm) spectra of CNCI crystals at room temperature. (c) Excitation wavelength-dependent PL spectra of CNCI crystals at room temperature. (d) Absorption spectrum of CNCI crystals; the inset shows the diffuse reflection spectrum of CNCI crystals. Excitation (e) and emission (f) wavelength-dependent PL and PLE spectra of CNCI crystals, respectively.

which means that one H_2O molecule is disordered over two sites. The disordered H_2O molecule has no H atoms in the model because they were not localized. Except for the H_2O molecule between the $(18\text{-crown-6})Na^+$ complex, each Na^+ connects with another H_2O molecule outside the complex to form sandwich-type $(18\text{-crown-6})_2Na_2(H_2O)_3^{2+}$ complex cations (Figure 1a). The basic synthon for all copper(I) halides was the rhombohedra with copper and halide atoms at alternate corners, which could be connected or fused by sharing corners or edges to form aggregates with higher unclarity.[29] Therefore, the Cu^+ ions are coordinated by three I^- ions forming CuI_3 triangles. These triangles are disordered over eight positions and connected with each other by edges and nodes forming a $Cu_4I_6^{2-}$ cluster (Figure 1b). There are two O−H···I hydrogen bonds, and the hydrogen-bond geometries in the CNCI structure are shown in Table S3. The main bond lengths in the CNCI structure are shown in Table S4. Finally, Figure 1c demonstrates the crystal structure of $(18\text{-crown-6})_2Na_2(H_2O)_3Cu_4I_6$ viewed along the *a*-axis to show the 0D character with isolated $Cu_4I_6^{2-}$ units.

High-quality green crystals are successfully prepared through a simple solution method, and the crystals exhibit strong green emission under blue light irradiation (Figure 2a). The PL and PLE spectra of CNCI crystals at room temperature are shown in Figure 2b. An ultra-broad-band excitation peak with a plateau covering the 300−500 nm range can be observed. Under excitation at 450 nm, it demonstrates a broad-band green emission, which is composed of a high-energy emission band at 536 nm and a tail in the lower-energy region (Figure 2b). The PLQY of the greenish-yellow emission is measured to

https://doi.org/10.1021/acs.chemmater.1c00085
Chem. Mater. 2021, 33, 4382−4389

be near unity (91.8%). The PL spectra recorded at different excitation wavelengths (365, 375, 395, 440, 450, and 460 nm) correspond to all of the available commercial LED chips, which are almost identical (Figure 2c), indicating its excellent commercial application prospects. Figure 2d shows the absorption spectrum of CNCI, which reveals an ultrabroad absorption band. According to the diffuse reflection spectrum, the calculated band gap of CNCI crystals is 2.43 eV, which is slightly smaller than those of other reported 0D Cu(I)-based organometallic halides.[30] In the present structure, the H_2O molecules and organic cations are connected by hydrogen bonding; thus, the orbitals between them are more or less hybridized. We propose that the orbital hybridization decreases the energy level of the valence band maximum (VBM) of the CNCI compound, and the decreased VBM leads to the smaller band gap of CNCI, as observed in other systems.[31] Moreover, it should be noted that the PL spectrum of CNCI crystals is not Gaussian symmetric but with a relatively long tail. The excitation wavelength-dependent PL spectra of CNCI crystals at room temperature are shown in Figure 2c,e. As the excitation wavelength varies from 450 to 300 nm, the PL peak positions remain unchanged, and the relative intensity of the low-energy tail becomes stronger. With the excitation wavelength further changing to 270 nm, a low-energy emission at 700 nm gradually appears (Figure 2e). To further investigate the dual emission of CNCI crystals, the emission wavelength-dependent PLE spectra of CNCI crystals are demonstrated in Figure 2f.

It turns out that the PLE spectrum monitored at 700 nm covers more broad edge in the short-wavelength region compared to that monitored at 536 nm, which corresponds to the dual emission when the excitation wavelength is reduced to 270 nm. The low-energy emission (700 nm) can be attributed to a CC excited state in the case of metal center interactions as reported previously,[29,32−34] which is also discussed in detail later.

To further understand the PL mechanism of CNCI crystals, low-temperature emission spectra, wavelength-dependent PL spectra, and the emission delay curve were investigated. The temperature-dependent PL spectra of CNCI crystals under 450 nm excitation are measured from 15 to 300 K. As shown in Figure 3a, with the decrease in temperature, the peak positions of this broad-band emission at 536 nm remain unchanged, and the full width at half-maximum (FWHM) of this broad-band emission gradually decreases from 120 to 54 nm; in addition, the PL of the low-energy tail almost disappears. The observed optical characteristics of CNCI crystals are similar to those of the Cu(I)-based metal halide cluster $Cu_4I_4(py)_4$ (py = pyridine) reported by the Ford group in 1993.[35] In addition, the Cu−Cu distance in CNCI (2.71 Å) is almost the same as the Cu−Cu distance (2.63−2.79 Å) in the reported CC and metal-to-ligand charge transfer (MLCT) or halide-to-ligand charge-transfer (HLCT) mechanisms. According to existing reports and models, it is difficult to accurately determine whether the high-energy emission is attributed to HLCT or MLCT; therefore, we think it is more reasonable to attribute it to MLCT/HLCT.[31] Figure 3b shows the PL spectra of CNCI crystals under different excitation wavelengths at room and low temperatures. Under excitation at 270 and 450 nm, low-energy emission at 700 nm can be observed both at 15 K and at 300 K. However, the relative intensity of the low-energy emission at 700 nm is weaker at low temperature under the same excitation. The fluorescence lifetime of the emission is

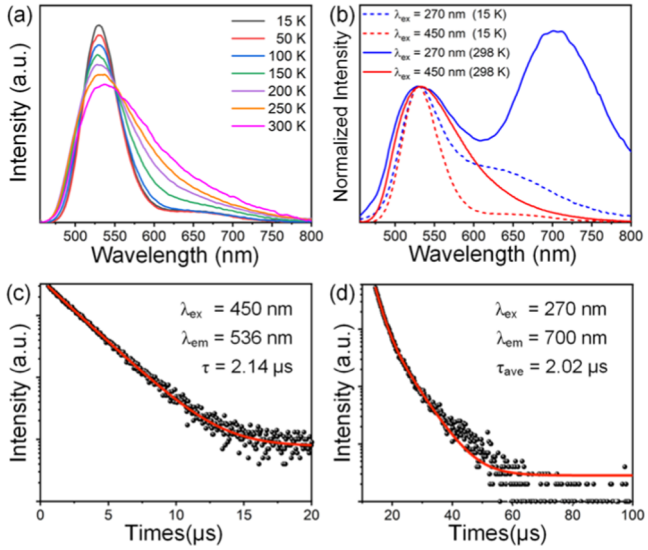

Figure 3. (a) Temperature-dependent PL spectra of CNCI crystals under 450 nm excitation. (b) Temperature- and excitation wavelength-dependent PL spectra of CNCI crystals. (c, d) Decay curve of CNCI crystals under different excitation and monitoring wavelengths at room temperature.

determined by time-resolved methods. Under excitation at 450 nm, monitoring at 536 nm, the lifetime of the CNCI crystals at room temperature is 2.14 μs based on single exponential-fitting (Figure 3c), which is similar to those of other low-dimensional metal halides.[36] Under excitation at 270 nm, monitoring at 700 nm, the average lifetime of the CNCI crystals is 2.02 μs based on double exponential-fitting (Figure 3d). The fluorescence lifetime can be calculated using eq 1[37]

$$\tau = A_1 \exp\left(\frac{-t}{\tau_1}\right) + A_2 \exp\left(\frac{-t}{\tau_2}\right) \quad (1)$$

and the average lifetimes are calculated using eq 2

$$\tau_{ave} = \frac{A_1\tau_1^2 + A_2\tau_2^2}{A_1\tau_1 + A_2\tau_2} \quad (2)$$

Due to the difference between the lifetimes monitored at 536 and 700 nm, the broad asymmetric emission bands with long tails can be attributed to two kinds of emitting centers. CC emission is generally observed in the region of 500−800 nm with lifetimes usually less than 20 μs,[38,39] and the spectral features allow us to attribute the observed luminescence at 700 nm to the CC excited state. Moreover, the PL intensity of CNCI exhibits linear dependence on the excitation power (Figure S2), ruling out the possibility that the emission originates from permanent defects, since the long-lived and finite defect states would be saturated at a high excitation power density.[40]

As is known, the luminescence properties of Cu(I)-based organometallic halides arise from a remarkable variety of emissive states, which have been extensively investigated in the last 30 years and can be summarized as follows: (a) low-energy emission, attributed to the CC excited state, can be observed in the case of metal center interactions and is independent of the nature of the ligands engaged in the complex and (b) high-energy emission is attributed to a MLCT/HLCT excited state.[29,32,33,39,41,42] Similarly, we propose a qualitative model for the mechanism of dual luminescence of CNCI based on the

https://doi.org/10.1021/acs.chemmater.1c00085
Chem. Mater. 2021, 33, 4382−4389

above experimental data and the existing model. The mechanism of dual luminescence of CNCI can be attributed to the synergistic effect of two energy states, a MLCT/HLCT excited state leading the high-energy emission at 536 nm and a CC excited state leading to low-energy emission at 700 nm, as shown in Figure 4. The effect of temperature on luminescence

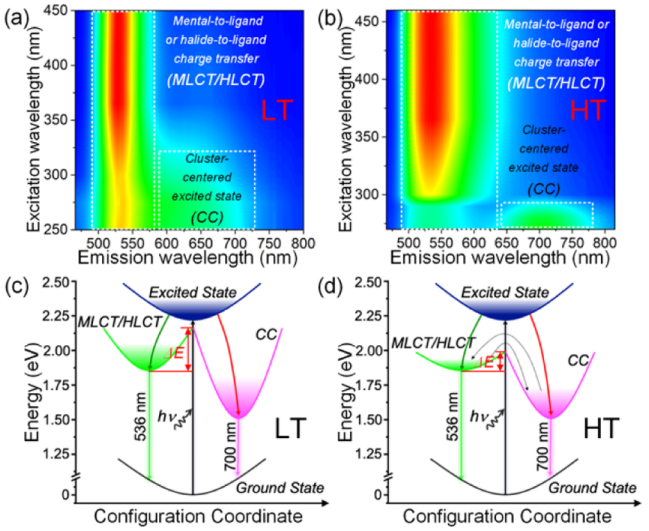

Figure 4. Consecutive PL/PLE correlation maps of CNCI (a) at a low temperature (LT, 15 K) and (b) at a high temperature (HT, 298 K). Schematic diagram of the emission mechanism at (c) LT and (d) HT.

can be followed with the consecutive PL/PLE correlation maps measured at different temperatures. Figure 4a,c shows the consecutive PL/PLE correlation maps and the schematic diagram of the emission mechanism of CNCI at 15 K. At low temperatures, the barrier height (ΔE) at the curve crossing is pretty high (Figure 4c) so that once the excitons relax into either state, the internal conversion rate is relatively slow to other photophysical processes, which leads to the relative weak intensity of the low-energy emission at 700 nm (Figures 3b and 4a). Figure 4b,d shows the consecutive PL/PLE correlation maps and the schematic diagram of the emission mechanism of CNCI at 298 K. At high temperatures, there is a relatively low ΔE at the curve crossing (Figure 4d) so that the two states are in thermal equilibrium. Due to the existence of thermal equilibrium, more excitons relax into the CC excited state compared to those at lower temperatures. Thus, the relative intensity of the low-energy emission at 700 nm at room temperature is stronger than that at low temperature.[35]

Stability is a key factor that affects the luminescence performance of the luminescence materials in LED applications. To further explore the chemical and moisture stability, CNCI was treated under extreme conditions of 85% relative humidity and at 85 °C. Figure S1 demonstrates the corresponding PL spectra depending on the aging time. The emission intensity of CNCI still maintains 78.4% of the pristine value over an aging time of 168 h (Figure 5b), which is exceptional among many reported organometallic halides.[43] Based on the excellent chemical and moisture stability, we mixed the powder of CNCI and the epoxy resin for three-dimensional (3D)-printing as mentioned above. The powder remains stable in the resin, and its luminous performance remains unchanged. We use a 3D printer to print small wafers of different thicknesses that fit the blue-emitting GaN chip. By choosing a suitable thickness of the wafers printed with CNCI and KSF:Mn^{4+} and packing them with a blue GaN chip, a WLED device can be fabricated (Figure 5a). Figure 5c presents the PL spectrum of the WLED device upon 20 mA drive

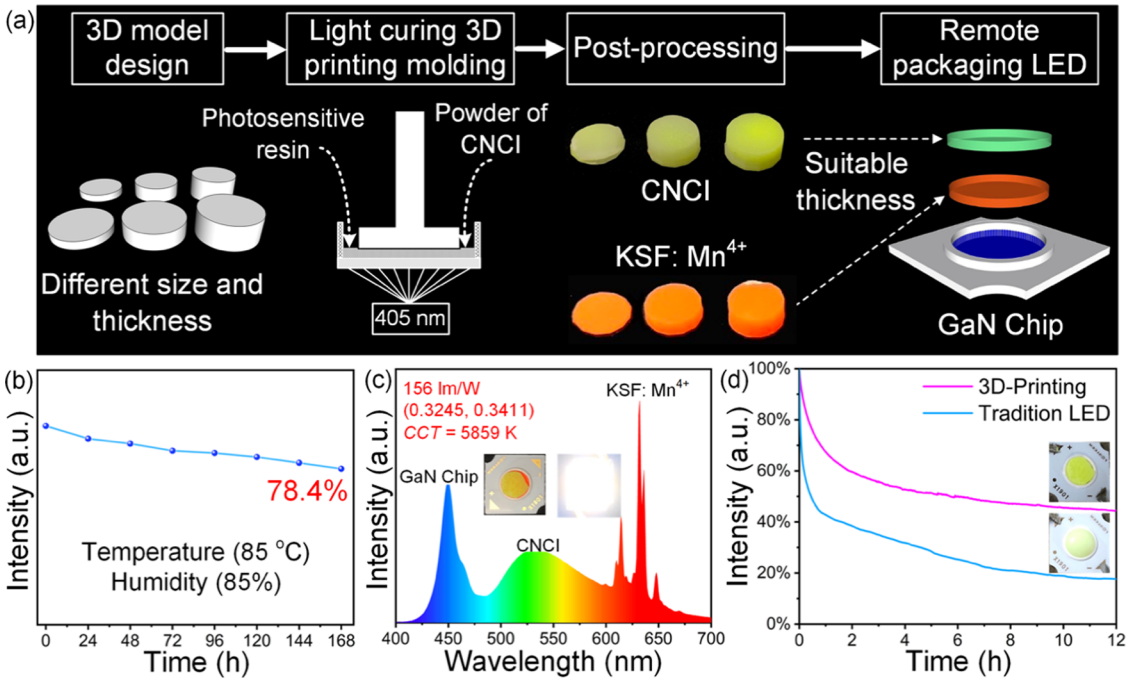

Figure 5. (a) Flow chart and the detailed fabrication process used in 3D-printing toward the package of the WLED device, which contains a GaN blue LED chip, red-emitting KSF:Mn^{4+}, and green-emitting CNCI wafers. (b) Time-dependent PL intensities of CNCI crystals over aging time of 168 h. (c) PL emission spectrum of the fabricated WLED device driven by 20 mA current. (d) Comparison of blue light stability of the LED device fabricated using 3D-printing with that of the LED fabricated using traditional methods.

https://doi.org/10.1021/acs.chemmater.1c00085
Chem. Mater. 2021, 33, 4382−4389

current, and the inset shows the photographs of the device when the current is turned on and off. The CIE color coordinate of the lit WLED device is (0.3245, 0.3411), with a CCT of 5859 K, a high color rendering index of 89.6, and high luminous efficacy of 156 lm/W at a drive current of 20 mA. Finally, we compare blue light stability of the LED device fabricated using a 3D printer with that of the LED fabricated using traditional methods (Figure 5d). It turns out that the LED device fabricated using a 3D printer shows excellent blue light stability. Compared with the LED fabricated using traditional methods, 3D-printing can encapsulate the material in resin in advance and then print out small wafers of appropriate size and thickness before fabricating the LED device. Due to the excellent chemical stability of CNCI, its luminescence in resin is not weakened, and the resin in turn has a certain protective effect on the material, resulting in its blue light stability being improved. The results suggest great potential of CNCI in solid-state lighting, and the newly purposed fabrication strategy involving 3D-printing delivers superior stability in practical applications.

CONCLUSIONS

In conclusion, a zero-dimensional Cu(I)-based organometallic halide, $(18\text{-crown-}6)_2Na_2(H_2O)_3Cu_4I_6$, with near-unity green light emission has been reported. The ultrabroad excitation band covering a 300−500 nm range and excellent chemical and moisture stability make CNCI crystals highly suitable for solid-state lighting application. The efficient green emission band centered at 536 nm with a tail at the lower-energy region was proved to be dual luminescence corresponding to two different energy states. The MLCT/HLCT excited state leads to high-energy emission at 536 nm, and a CC excited state leads to low-energy emission at 700 nm. The as-prepared high-performance LED device fabricated with a 3D printer demonstrates great potential in solid-state lighting. Our work provides the design principle of new low-dimensional luminescent metal halides with ultra-broad-band-excitable characteristics and demonstrates potentials in the WLED fields.

ASSOCIATED CONTENT

Supporting Information

The Supporting Information is available free of charge at https://pubs.acs.org/doi/10.1021/acs.chemmater.1c00085.

X-ray crystallographic data for $(18\text{-crown-}6)_2Na_2(H_2O)_3Cu_4I_6$ (CIF)

Crystallographic details; Rietveld refinement; and additional PL data (PDF)

AUTHOR INFORMATION

Corresponding Author

Zhiguo Xia − *The State Key Laboratory of Luminescent Materials and Devices, Guangdong Provincial Key Laboratory of Fiber Laser Materials and Applied Techniques, School of Materials Science and Engineering, South China University of Technology, Guangzhou 510641, China;* orcid.org/0000-0002-9670-3223; Email: xiazg@scut.edu.cn

Authors

Jinglong Huang − *The State Key Laboratory of Luminescent Materials and Devices, Guangdong Provincial Key Laboratory of Fiber Laser Materials and Applied Techniques, School of Materials Science and Engineering, South China University of Technology, Guangzhou 510641, China*

Binbin Su − *The State Key Laboratory of Luminescent Materials and Devices, Guangdong Provincial Key Laboratory of Fiber Laser Materials and Applied Techniques, School of Materials Science and Engineering, South China University of Technology, Guangzhou 510641, China*

Enhai Song − *The State Key Laboratory of Luminescent Materials and Devices, Guangdong Provincial Key Laboratory of Fiber Laser Materials and Applied Techniques, School of Materials Science and Engineering, South China University of Technology, Guangzhou 510641, China*

Maxim S. Molokeev − *Laboratory of Crystal Physics, Kirensky Institute of Physics, Federal Research Center KSC SB RAS, Krasnoyarsk 660036, Russia; Siberian Federal University, Krasnoyarsk 660041, Russia; Research and Development Department, Kemerovo State University, Kemerovo 650000, Russia;* orcid.org/0000-0002-8297-0945

Complete contact information is available at: https://pubs.acs.org/10.1021/acs.chemmater.1c00085

Author Contributions

⊥J.H. and B.S. contributed equally to this work.

Notes

The authors declare no competing financial interest.

ACKNOWLEDGMENTS

This research was supported by the National Natural Science Foundation of China (Grant Nos. 51961145101 and 51972118), the Fundamental Research Funds for the Central Universities (D2190980), the Guangzhou Science and Technology Project (202007020005), International Cooperation Project of National Key Research and Development Program of China (2021YFE0105700), and the Local Innovative and Research Teams Project of Guangdong Pearl River Talents Program (2017BT01X137). The reported study was also funded by RFBR according to research project no. 19-52-80003.

REFERENCES

(1) Zhao, M.; Zhang, Q. Y.; Xia, Z. G. Structural Engineering of Eu^{2+}-Doped Silicates Phosphors for LED Applications. *Acc. Mater. Res.* **2020**, *1*, 137−145.

(2) Li, M. Z.; Xia, Z. G. Recent progress of Zero-Dimensional Luminescent Metal Halides. *Chem. Soc. Rev.* **2021**, *50*, 2626−2662.

(3) Lin, Y. C.; Bettinelli, M.; Karlsson, M. Unraveling the Mechanisms of Thermal Quenching of Luminescence in Ce^{3+}-Doped Garnet Phosphors. *Chem. Mater.* **2019**, *31*, 3851−3862.

(4) Zhou, G. J.; Su, B. B.; Huang, J. L.; Zhang, Q. Y.; Xia, Z. G. Broad-band emission in metal halide perovskites: Mechanism, materials, and applications. *Mater. Sci. Eng., R* **2020**, *141*, No. 100548.

(5) Cao, D. H.; Stoumpos, C. C.; Farha, O. K.; Hupp, J. T.; Kanatzidis, M. G. 2D Homologous Perovskites as Light-Absorbing Materials for Solar Cell Applications. *J. Am. Chem. Soc.* **2015**, *137*, 7843−50.

(6) Li, L. N.; Sun, Z. H.; Wang, P. D.; Hu, W.; Wang, S. S.; Ji, C. M.; Hong, M. C.; Luo, J. H. Tailored Engineering of an Unusual $(C_4H_9NH_3)_2(CH_3NH_3)_2Pb_3Br_{10}$ Two-Dimensional Multilayered Perovskite Ferroelectric for a High-Performance Photodetector. *Angew. Chem., Int. Ed.* **2017**, *56*, 12150−12154.

(7) Zhou, G. J.; Liu, Z. Y.; Huang, J. L.; Molokeev, M. S.; Xiao, Z. W.; Ma, C. G.; Xia, Z. G. Unraveling the Near-Unity Narrow-Band Green Emission in Zero-Dimensional Mn^{2+}-Based Metal Halides: A

Case Study of $(C_{10}H_{16}N)_2Zn_{1-x}Mn_xBr_4$ Solid Solutions. *J. Phys. Chem. Lett.* **2020**, *11*, 5956−5962.
(8) Su, B. B.; Zhou, G. J.; Huang, J. J.; Song, E. H.; Nag, A.; Xia, Z. G. Mn^{2+}-Doped Metal Halide Perovskites: Structure, Photoluminescence, and Application. *Laser Photonics Rev.* **2020**, *15*, No. 200334.
(9) Li, M. Z.; Zhou, J.; Zhou, G. J.; Molokeev, M. S.; Zhao, J.; Morad, V.; Kovalenko, M. V.; Xia, Z. G. Hybrid Metal Halides with Multiple Photoluminescence Centers. *Angew. Chem., Int. Ed.* **2019**, *58*, 18670−18675.
(10) Du, P.; Luo, L. H.; Cheng, W. Neoteric Mn^{2+}-activated $Cs_3Cu_2I_5$ dazzling yellow-emitting phosphors for white-LED. *J. Am. Ceram. Soc.* **2020**, *103*, 1149−1155.
(11) Cortecchia, D.; Dewi, H. A.; Yin, J.; Bruno, A.; Chen, S.; Baikie, T.; Boix, P. P.; Gratzel, M.; Mhaisalkar, S.; Soci, C.; Mathews, N. Lead-Free $MA_2CuCl_xBr_{4-x}$ Hybrid Perovskites. *Inorg. Chem.* **2016**, *55*, 1044−1052.
(12) Jun, T.; Sim, K.; Iimura, S.; Sasase, M.; Kamioka, H.; Kim, J.; Hosono, H. Lead-Free Highly Efficient Blue-Emitting Cs_3 Cu_2I_5 with 0D Electronic Structure. *Adv. Mater.* **2018**, *30*, No. 1804547.
(13) Lian, L. Y.; Zheng, M. Y.; Zhang, P.; Zheng, Z.; Du, K.; Lei, W.; Gao, J. B.; Niu, G. D.; Zhang, D. L.; Zhai, T. Y.; Jin, S. Y.; Tang, J.; Zhang, X. W.; Zhang, J. B. Photophysics in $Cs_3Cu_2X_5$ (X = Cl, Br, or I): Highly Luminescent Self-Trapped Excitons from Local Structure Symmetrization. *Chem. Mater.* **2020**, *32*, 3462−3468.
(14) Creason, T. D.; McWhorter, T. M.; Bell, Z.; Du, M. H.; Saparov, B. K_2CuX_3 (X = Cl, Br): All-Inorganic Lead-Free Blue Emitters with NearUnity Photoluminescence Quantum Yield. *Chem. Mater.* **2020**, *32*, 6197−6205.
(15) Yue, C. Y.; Sun, C.; Li, D. Y.; Dong, Y. H.; Wang, C. L.; Zhao, H. F.; Jiang, H.; Jing, Z. H.; Lei, X. W. Organic-Inorganic Hybrid Heterometallic Halides with Low-Dimensional Structures and Red Photoluminescence Emissions. *Inorg. Chem.* **2019**, *58*, 10304−10312.
(16) Zhou, C. K.; Lee, S. J.; Lin, H. R.; Neu, J.; Chaaban, M.; Xu, L. J.; Arcidiacono, A.; He, Q.; Worku, M.; Ledbetter, L.; Lin, X. S.; Schlueter, J. A.; Siegrist, T.; Ma, B. W. Bulk Assembly of Multicomponent Zero-Dimensional Metal Halides with Dual Emission. *ACS Mater. Lett.* **2020**, *2*, 376−380.
(17) Xu, L. J.; Lee, S.; Lin, X. S.; Ledbetter, L.; Worku, M.; Lin, H.; Zhou, C.; Liu, H. R.; Plaviak, A.; Ma, B. W. Multicomponent Organic Metal Halide Hybrid with White Emissions. *Angew. Chem., Int. Ed.* **2020**, *132*, 14320−14123.
(18) Mao, L. L.; Guo, P. J.; Kepenekian, M.; Hadar, I.; Katan, C.; Even, J.; Schaller, R. D.; Stoumpos, C. C.; Kanatzidis, M. G. Structural Diversity in White-Light-Emitting Hybrid Lead Bromide Perovskites. *J. Am. Chem. Soc.* **2018**, *140*, 13078−13088.
(19) Zhao, L. F.; Lin, Y. L.; Kim, H.; Giebink, N. C.; Rand, B. P. Donor/Acceptor Charge-Transfer States at Two-Dimensional Metal Halide Perovskite and Organic Semiconductor Interfaces. *ACS Energy Lett.* **2018**, *3*, 2708−2712.
(20) Hu, H. W.; Meier, F.; Zhao, D. M.; Abe, Y.; Gao, Y.; Chen, B. B.; Salim, T.; Chia, E. E. M.; Qiao, X. F.; Deibel, C.; Lam, Y. M. Efficient Room-Temperature Phosphorescence from Organic-Inorganic Hybrid Perovskites by Molecular Engineering. *Adv. Mater.* **2018**, No. 1707621.
(21) Li, S.; Xu, J.; Li, Z. G.; Zeng, Z. G.; Li, W.; Cui, M. H.; Qin, C. C.; Du, Y. P. One-Dimensional Lead-Free Halide with Near-Unity Greenish-Yellow Light Emission. *Chem. Mater.* **2020**, *32*, 6525−6531.
(22) Nurtaeva, A.; Holt, E. M. Aqua(benzo-15-crown-5)lithium-hexa-μ-iodotetracoopper-benzo-15-crown-5 (2/1/2), bis[bis(benzo-15-crown-5)caesium] hexa-μiodotetracopper and μ-aqua-bis[aqua-(18-crown-6)sodium] hexa-μ- iodotetracoppert. *Acta Cryst.* **1999**, *C55*, 1453−1457.
(23) Sheldrick, G. M. A short history of SHELX. *Acta Cryst.* **2008**, *64*, 112−122.
(24) *PLATON − A Multipurpose Crystallographic Tool*; Utrecht University: Utrecht, The Netherlands, 2008.
(25) *Bruker, Topas. General Profile and Structure Analysis Software for Powder Diffraction Data, version 4*; Bruker AXS: Karlsruhe: Germany, 2008.
(26) Rath, N. P.; Holt, E. M. Copper(i) Iodide Complexes of Novel Structure: $[Cu_4I_6][Cu_8I_{13}]K_7$(12-crown-4)$_6$, $[Cu_4I_6]K_2$(15-crown-5)$_2$, and $[Cu_3I_4]$K(dibenzo-24-crown-8). *J. Chem. Soc., Chem. Commun.* **1985**, *55*, 665−667.
(27) Morad, V.; Yakunin, S.; Kovalenko, M. V. Supramolecular Approach for Fine-Tuning of the Bright Luminescence from Zero-Dimensional Antimony(III) Halides. *ACS Mater. Lett.* **2020**, *2*, 845−852.
(28) Merzlyakova, E.; Wolf, S.; Lebedkin, S.; Bayarjargal, L.; Neumeier, B. L.; Bartenbach, D.; Holzer, C.; Klopper, W.; Winkler, B.; Kappes, M.; Feldmann, C. 18-Crown-6 Coordinated Metal Halides with Bright Luminescence and Nonlinear Optical Effects. *J. Am. Chem. Soc.* **2021**, *143*, 798−804.
(29) Peng, R.; Li, M.; Li, D. Copper(I) halides: A versatile family in coordination chemistry and crystal engineering. *Coord. Chem. Rev.* **2010**, *254*, 1−18.
(30) Liu, W.; Fang, Y.; Wei, G. Z.; Teat, S. J.; Xiong, K. C.; Hu, Z. C.; Lustig, W. P.; Li, J. A Family of Highly Efficient CuI-Based Lighting Phosphors Prepared by a Systematic, Bottom-up Synthetic Approach. *J Am. Chem. Soc.* **2015**, *137*, 9400−9408.
(31) Song, G. M.; Li, M. Z.; Zhang, S. Z.; Wang, N. Z.; Gong, P. F.; Xia, Z. G.; lin, Z. S. Enhancing Photoluminescence Quantum Yield in 0D Metal Halides by Introducing Water Molecules. *Adv. Funct. Mater.* **2020**, *30*, No. 2002468.
(32) Braga, D.; Grepioni, F.; Maini, L.; Mazzeo, P. P.; Ventura, B. Solid-state reactivity of copper(i) iodide: luminescent 2D-coordination polymers of CuI with saturated bidentate nitrogen bases. *New J. Chem.* **2011**, *35*, 339−344.
(33) Perruchas, S.; Tard, C.; Le Goff, X. F.; Fargues, A.; Garcia, A.; Kahlal, S.; Saillard, J. Y.; Gacoin, T.; Boilot, J. P. Thermochromic luminescence of copper iodide clusters: the case of phosphine ligands. *Inorg. Chem.* **2011**, *50*, 10682−11692.
(34) Mazzeo, P. P.; Maini, L.; Petrolati, A.; Fattori, V.; Shankland, K.; Braga, D. Phosphorescence quantum yield enhanced by intermolecular hydrogen bonds in Cu_4I_4 clusters in the solid state. *Dalton Trans.* **2014**, *43*, 9448−9455.
(35) Ryu, C. K.; Vitale, M.; Ford, P. C. Photoluminescence properties of the structurally analogous tetranuclear copper(I) clusters Cu_4X_4(dpmp)$_4$ (X = I, Br, Cl; dpmp = 2-(diphenylmethyl)pyridine). *Inorg. Chem.* **1993**, *32*, 869−874.
(36) Su, B. B.; Song, G. M.; Molokeev, M. S.; Lin, Z. H.; Xia, Z. G. Synthesis, Crystal Structure and Green Luminescence in Zero-Dimensional Tin Halide $(C_8H_{14}N_2)_2SnBr_6$. *Inorg. Chem.* **2020**, *59*, 9962−9968.
(37) Liu, Y.; Rong, X. M.; Li, M. Z.; Molokeev, M. S.; Zhao, J.; Xia, Z. G. Incorporating Rare-Earth Terbium(III) Ions into Cs2 AgInCl6:Bi Nanocrystals toward Tunable Photoluminescence. *Angew. Chem., Int. Ed.* **2020**, *59*, 11634−11640.
(38) Kyle, K. R.; Ryu, C. K.; DiBenedetto, J. A.; Ford, P. C. Photophysical Studies in Solution of the Tetranuclear $Cu_4I_4L_4$ (L = Pyridine or Substituted Copper(I) Clusters Pyridine)$^{1-3}$. *J. Am. Chem. Soc.* **1991**, *113*, 2954−2965.
(39) Ford, P. C.; Cariati, E.; Bourassa, J. Photoluminescence Properties of Multinuclear Copper(I) Compounds. *Chem. Rev.* **1999**, *99*, 3625−3647.
(40) Wu, G. H.; Zhou, C. K.; Ming, W. M.; Han, D.; Chen, S. Y.; Neu, J.; Siegris, T.; Neu, J.; Siegrist, T.; Du, M. H.; Ma, B. W.; et al. A One-Dimensional Organic Lead Chloride Hybrid with Excitation-Dependent Broadband Emissions. *ACS Energy Lett.* **2018**, *3*, 1443−1449.
(41) Perruchas, S.; Goff, X.; Maron, S.; Maurin, I.; Guillen, F.; Garcia, A.; Gacoin, T.; Boilot, J. P. Mechanochromic and Thermochromic Luminescence of a Copper Iodide Cluster. *J. Am. Chem. Soc.* **2010**, *132*, 10967−10969.
(42) Braga, D.; Maini, L.; Mazzeo, P. P.; Ventura, B. Reversible interconversion between luminescent isomeric metal-organic frameworks of $[Cu_4I_4(DABCO)_2]$ (DABCO = 1,4-diazabicyclo[2.2.2]-octane). *Chem. - Eur. J.* **2010**, *16*, 1553−1559.

https://doi.org/10.1021/acs.chemmater.1c00085
Chem. Mater. 2021, 33, 4382−4389

(43) Zhao, M.; Liao, H. X.; Ning, L. X.; Zhang, Q. Y.; Liu, Q. L.; Xia, Z. G. Next-Generation Narrow-Band Green-Emitting $RbLi(Li_3SiO_4)_2:Eu^{2+}$ Phosphor for Backlight Display Application. *Adv. Mater.* **2018**, *30*, No. 1802489.

https://doi.org/10.1021/acs.chemmater.1c00085
Chem. Mater. 2021, 33, 4382−4389